Communicated by Dr Zhang Tao

# Journal Pre-proof

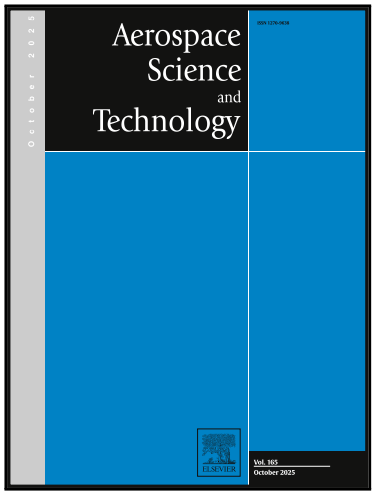


A novel scenario of two-impulse Moon-Planet transfer

Vladimir S. Aslanov

PII: S1270-9638(25)01321-5
DOI: https://doi.org/10.1016/j.ast.2025.111258
Reference: AESCTE 111258

To appear in: *Aerospace Science and Technology*

Received date: 20 August 2025
Revised date: 7 October 2025
Accepted date: 8 November 2025

Please cite this article as: Vladimir S. Aslanov , A novel scenario of two-impulse Moon-Planet transfer, *Aerospace Science and Technology* (2025), doi: https://doi.org/10.1016/j.ast.2025.111258

Highlights

- Space elevator consists of a space station and a climber
- Dynamics of a space elevator from Phobos to Mars is studied
- Motion is considered within the context of a planar elliptic RTBP
- The climber's motion law is chosen so that the tether tightens
- It is proven that oscillations are damped when the space elevator is deployed

# A novel scenario of two-impulse Moon-Planet transfer

Vladimir S. Aslanov[1]

*Moscow Aviation Institute (National Research University), 4, Volokolamskoe shosse, Moscow, A-80, GSP-3, 125993, Russia*

**Abstract**

The paper proposes a new scenario of two-impulse Moon-Planet transfer. The acceleration impulse is applied when the spacecraft starts from the moon's surface and the braking impulse is applied when the spacecraft reaches a predefined point on the line connecting the centers of mass of the planet and the moon. After that, the spacecraft free-falls to the planet's surface. The equations of motion in the framework of the planar elliptic restricted three-body problem and the planet atmospheric entry dynamic equations are used to model the spacecraft motion. Numerical simulations for arbitrarily chosen trajectories demonstrate the feasibility of the new scenario for two-impulse Phobos-Mars and Moon-Earth transfers. For the Earth-Moon system, the total velocity increment for the proposed two-impulse transfer flight is comparable and the Moon-Earth transfer time is reduced by more than half compared to a traditional transfer that involves a near-lunar orbit.

*Keywords: Moon-Planet transfer; two impulses; planar elliptic RTBP; Phobos to Mars; Moon to Earth.*

## 1. Introduction

More than 50 years ago, the United States and the Soviet Union began active lunar exploration, marking the start of the Lunar Race. The most notable missions of the 20th century were the Apollo and Luna programs, which involved exploring

[1] E-mail address: aslanov_vs@mail.ru.

the Moon's surface using rovers and delivering lunar samples to Earth. Interest in lunar exploration has grown considerably over the past decade, with China, the European Union, India, Japan, and other countries joining the Lunar Race. The theoretical justification of lunar missions has been the subject of many articles (e.g. [1–22]), which consider all stages of transfer between Earth and the Moon. One important phase of future lunar missions will be delivering lunar samples from the surface of the Moon to Earth via Moon-Earth return trajectories, which typically involve near-lunar orbits. In this case, new scenarios for delivering lunar samples to Earth will be needed to enable return trajectories offering advantages such as ease of implementation, reduced transport time, and lower fuel costs. New scenarios can be considered as an alternative to existing ones, involving the use of impulse Hohmann transfers and low thrust.

In cases where motion occurs solely within the gravitational field of a planet or moon, that is within the framework of the restricted two-body problem, two- and three-impulse trajectories are energetically efficient. For a coplanar transfer between two circular orbits, the Hohmann transfer is energetically efficient [23]. However, in transfers between a near-planetary orbit and a lunar orbit (or vice versa), the task of identifying energetically efficient trajectories becomes significantly more complex, as the problem must be analyzed within the framework of the restricted three-body problem. In such cases, the Hohmann transfer is no longer optimal. Multi-impulse Moon-Earth transfer scheme is proposed in [7]. In [9, 10] two- and three-burn transfers are considered for flights between planetary moons. The Moon-to-Moon Analytical Transfer (MMAT) method is used to compute the required impulses. This approximate technique, described in [11], is based on the circular restricted three-body problem in inter-moon space and the two-body problem in the vicinity of each moon. In [8], the differential correction approach was used to construct an optimization algorithm for a two-impulse transfer from the Earth to the Moon within the framework of the circular restricted three-body problem. The results of numerical modeling show that the two-impulse transfer obtained as a result of optimization needs less energy than the Hohmann transfers.

This paper aims to substantiate the feasibility of a simple two-impulse transfer scenario from a moon's surface to a planet's surface, and to estimate the transfer time and total velocity impulse using two systems as examples: Phobos–Mars and Moon–Earth. The problem is considered in the framework of the planar elliptic restricted three-body problem.

## 2. Basic idea of the method

The idea for this work arose from the issue [24], in which a space elevator delivers a probe from Phobos to a given point on the line connecting the centers of mass of Mars and Phobos. The probe then separates from the space elevator, after which it either falls to the surface of Mars or begins to rotate around it. The probe can also be delivered to the given point using a two-impulse transfer similar to the Hohmann transfer. The first acceleration impulse is given to the probe at the start from the surface of Phobos, and the second braking impulse is carried out when the probe reaches the given position on the line connecting the centers of mass of Mars and Phobos.

Consider the planar restricted circular three-body problem in the Local-Vertical-Local-Horizontal (LVLH) frame $Oxy$, whose origin $O$ is the center of mass of the planet-moon system (Fig. 1). The points $M_1$ and $M_2$ shown in Fig. 1 are the centers of mass of the planet and the moon, respectively. Any material point initially at relative rest ($\dot{x}=0, \dot{y}=0$) on the line connecting the centers of mass of the primaries (point $A_2$ in Fig.1), within a rotating frame $Oxy$, will undergo one of three possible types of motion due to the gravitational attraction of these primaries:

1) motion around a planet (1 primary)

$$x_{L_3} < x_{A_2} < x_{L_1}; \tag{1}$$

2) motion around a moon (1 primary)

$$x_{L_1} < x_{A_2} < x_{L_2}; \tag{2}$$

3) motion around the planet and the moon along the outer trajectory when the planet and the moon remain inside the area bounded by the 3 body trajectory

$$x_{A_2} > x_{L_2} \wedge x_{A_2} < x_{L_3}, \tag{3}$$

where $x_i$ is the coordinate of the *i* point in the frame $Oxy$. Only the three collinear libration points ($L_1$, $L_2$, and $L_3$), which are equilibrium positions, are the exceptions.

We are only interested in the trajectory that originates on the moon's surface and terminates on the planet's surface. Let us divide this trajectory into two sections (Fig. 1): the section $A_1A_2$ (launch trajectory) from the launch point $A_1$ on the moon's surface to the transition point on the axis $Ox$, and the section $A_2A_3$ (landing trajectory) from the transition point $A_2$ to the landing point $A_3$ on the planet's surface. Consider first the $A_2A_3$ section. Suppose that the transition point $A_2$ lies between the $L_1$ collinear libration point and the centre of mass of the planet $M_1$

$$x_{M_1} < x_{A_2} < x_{L_1}, \tag{4}$$

where $x_{M_1} = -\mu r$ is the coordinate of the $M_1$ point in LVLH frame, $\mu = \dfrac{m_2}{m_1 + m_2}$ is the mass ratio, $r$ is the distance between the two primaries. In this case, the spacecraft moves along trajectories within which the planet, or rather its center of mass, is always placed. It is possible to choose the transition point $A_2$ such that the spacecraft's trajectory crosses the planet's surface.

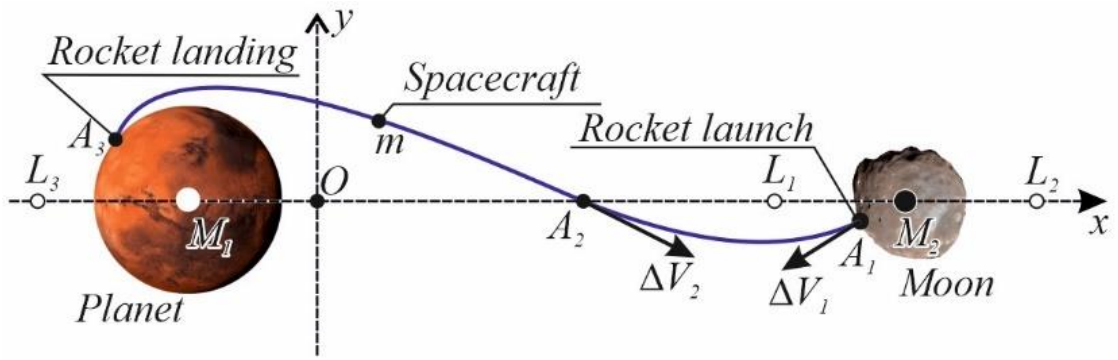


**Fig. 1.** The two-impulse Moon-Planet transfer in the frame $Oxy$.

The example of the Mars-Phobos system shows how the position of the transition point $A_2$ affects the landing trajectory when the spacecraft is either rotating around Mars (Fig. 2a) or falling on the surface of Mars (Fig. 2b). The landing trajectory to Mars is shown without taking into account aerodynamic forces. Classical equations of motion in terms of the planar elliptic restricted three-body problem [25] in the LVLH frame $Oxy$ are used to construct trajectories. These equations are given below in Section 3.

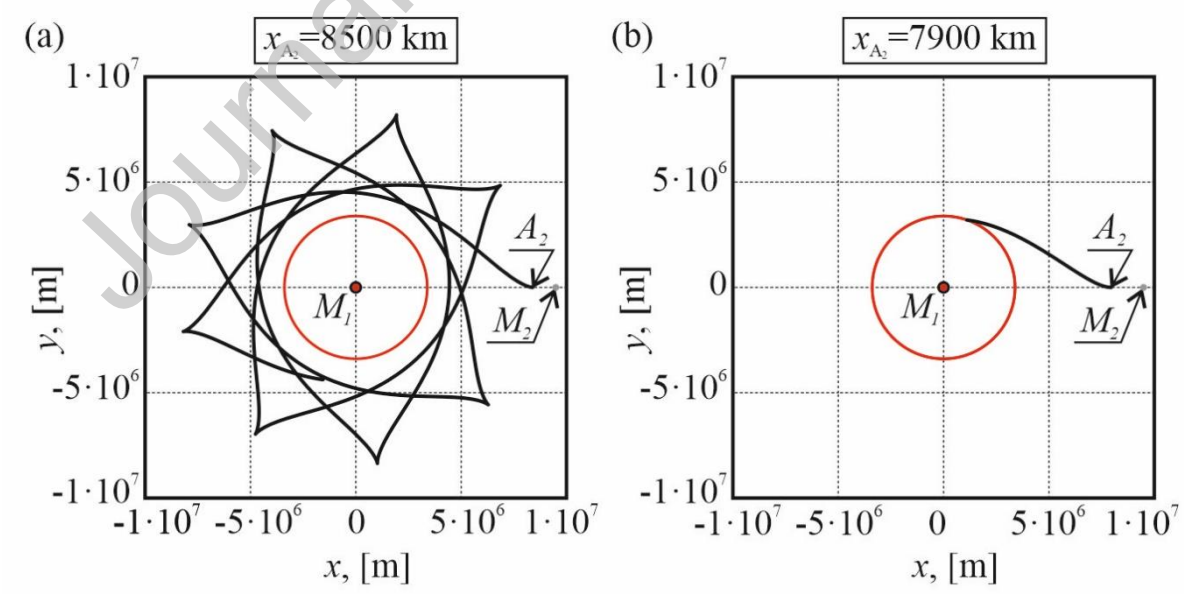


**Fig. 2.** Spacecraft trajectories (red curve is the Mars surface, black curve is the trajectory, grey curve is the Phobos surface).

Now the question remains: How can a spacecraft get from a moon's surface to the transition point $A_2$? To do this, it is sufficient to provide the first acceleration velocity impulse $\Delta V_1$ (required velocity increment) of the spacecraft at the launch point on the moon's surface and the second deceleration impulse $-\Delta V_2$ (required velocity reduction) at the transition point $A_2$. The next step is to select the launch point $A_1$ for the spacecraft, and the magnitude and direction of the acceleration and deceleration impulses. Finally, if the planet has an atmosphere, the aerodynamic force should be considered at the end of the second part of the transfer.

## 3. Equations of Motion

This section contains three mathematical models of the spacecraft motion that are required for modeling the proposed two-impulse Moon-Planet transfers.

1. Classical equations of motion in terms of the planar elliptic restricted three-body problem [25] in the LVLH frame $Oxy$ are used to describe the motion from the transition point $A_2$ to an atmospheric boundary or to a planet surface (if there is no atmosphere). These equations can be used to obtain a new system of equations by the method of backward integration [26, 27] to describe the launch trajectory, allowing us to obtain backward trajectories from the transition point $A_2$ to the launch point $A_1$ on the moon's surface.

2. In the case of a small moon (e.g. the Mars-Phobos system) when it can be assumed that the center of mass of a planet coincides with the origin of the LVLH frame $Oxy$. In this case the classical equations of motion are used in the context of the restricted planar elliptic three-body problem with the addition of the aerodynamic force to describe the motion of spacecraft taking into account the influence of the planet’s atmosphere.

3. On the contrary, in the case of a large moon (the Earth-Moon system), special equations of motion for the spacecraft in the atmosphere are required. The reentry equations are applied assuming that the planet's rotation is negligible [28, 29].

*3.1. Equations of motion in the planar elliptic restricted three-body problem*

Consider the equations of motion of a mass point in gravitational fields of two primaries in the LVLH frame $Oxy$ (Fig. 1) within the scope of the planar elliptic restricted three-body problem [25]

$$\ddot{x} - \dot{f}^2 x - 2\dot{f}\,\dot{y} - \ddot{f}\,y = \frac{\partial U}{\partial x}, \tag{5}$$

$$\ddot{y} - \dot{f}^2 y + 2\dot{f}\,\dot{x} + \ddot{f}\,x = \frac{\partial U}{\partial y}, \tag{6}$$

where $x$, $y$ is the mass point's coordinates, $f$ is the true anomaly, the dot denotes the time derivative. The second, third, and fourth terms on the left-hand side of equations (5) and (6) represent the components of the centrifugal, Coriolis, and rotational accelerations arising from the motion of the non-inertial coordinate system $Oxy$. The potential $U$ of Eqs. (5) and (6) is written as

$$U(x,y) = G\left(\frac{m_1}{r_1} + \frac{m_2}{r_2}\right), \tag{7}$$

where $G$ is Newtonian gravitational constant, the distances between the primaries (1 and 2) and the spacecraft is defined as (Fig. 1)

$$r_1 = \sqrt{(x+\mu r)^2 + y^2}, \qquad r_2 = \sqrt{(x-(1-\mu)r)^2 + y^2}. \tag{8}$$

The distance between the two primaries is

$$r = \frac{p}{1 + e\cos f}, \tag{9}$$

where $p = a(1-e^2)$ is the semilatus rectum, $e$ is the eccentricity of the orbit of the primaries, and $a$ is the semi-major axis of an elliptical orbit. The time derivative of the true anomaly is given by [25]

$$\dot{f} = \frac{c}{r^2}, \tag{10}$$

where $c = \sqrt{G(m_1 + m_2)p}$ .

*3.2. Equations of motion in the planar elliptic restricted three-body problem with consideration of aerodynamic force*

In the case of a small moon, the distance between the center of mass of the planet $M_1$ and the center of mass of the planet-moon system $O$ is much smaller than the radius of the planet (Fig. 1). For example, this distance $d = \mu r$ is minuscule ($\mu r < 0.161$ m) in the Mars-Phobos system, for which $\mu = 1.67 \times 10^{-8}$. In this case, it can be supposed that the centers of mass of the planet and the planet-moon system coincide. The LVLH frame $Oxyz$ rotates with angular velocity $\dot{f} = \frac{df}{dt}$ relative to the fixed frame $M_1XYZ$ (Fig. 3). It is also assumed the planet does not rotate relative to the frame $M_1XYZ$. To take into account the influence of the atmosphere on the spacecraft, the equations of motion (5) and (6) are used with the addition of the aerodynamic force. Assume that the spacecraft's motion in a planetary atmosphere is additionally affected only by drag,

$$D = C_D qA, \tag{11}$$

where $\rho$ is a planet atmospheric density, $C_{\mathrm{D}}$ is the aerodynamic drag coefficient, $A$ is the cross-section of spacecraft, and $q=\dfrac{\rho V^2}{2}$ is the dynamic pressure. A planet atmospheric density can be defined as

$$\rho=\rho_0 e^{-h/h_{\mathrm{s}}}, \tag{12}$$

where $\rho_0$ is the planet's surface atmospheric density, $h$ is the spacecraft's altitude, $h_{\mathrm{s}}$ is the scale height.

Suppose that the points $M_1$ and $O$ coincide (Fig. 1), and note that the drag force is in the opposite direction to the spacecraft's velocity vector

$$\mathbf{D}=-C_{\mathrm{D}}A\frac{\rho V\mathbf{V}}{2}, \tag{13}$$

where the velocity vector $\mathbf{V}$ can be calculated as the sum of the translational velocity $\mathbf{V}_{\mathrm{e}}$ and the relative velocity $\mathbf{V}_{\mathrm{r}}$

$$\mathbf{V}=\mathbf{V}_{\mathrm{e}}+\mathbf{V}_{\mathrm{r}}, \tag{14}$$

$$\mathbf{V}_{\mathrm{e}}=R\dot{f}\,(-\sin\alpha,\cos\alpha)^T,\ \mathbf{V}_{\mathrm{r}}=(\dot{x},\dot{y})^T. \tag{15}$$

From the geometry of the system (Fig. 3), the following relationships follow:

$$R=\sqrt{x^2+y^2},\ \tan\beta=\frac{\dot{y}+R\dot{f}\cos\alpha}{\dot{x}-R\dot{f}\sin\alpha},\ \tan\alpha=\frac{y}{x},\quad h=R-R_0, \tag{16}$$

where $R_0$ is the planet's radius.

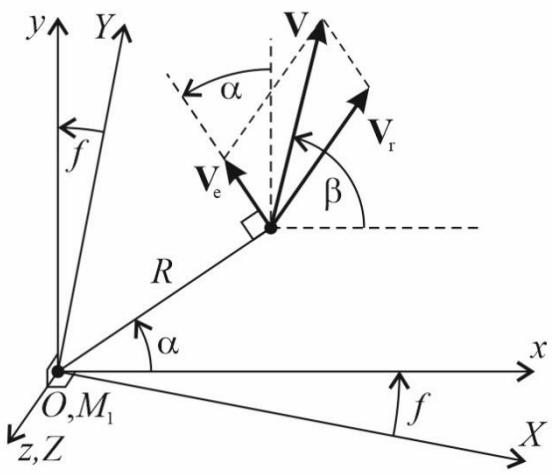


**Fig. 3.** The frames $Oxyz$ and $M_1XYZ$.

The equations of motion of the spacecraft in the planetary atmosphere can be written using formulas (13)-(16) as

$$\ddot{x} - \dot{f}^2 x - 2\dot{f}\,\dot{y} - \ddot{f}\,y = -\frac{C_D S}{m}\frac{\rho V^2}{2}\cos\beta + \frac{\partial U}{\partial x}, \tag{17}$$

$$\ddot{y} - \dot{f}^2 y + 2\dot{f}\,\dot{x} + \ddot{f}\,x = -\frac{C_D S}{m}\frac{\rho V^2}{2}\sin\beta + \frac{\partial U}{\partial y}. \tag{18}$$

*3.3. The planet atmospheric entry dynamic equations*

Under the assumption that the planet's rotation is negligible, the planet atmospheric entry dynamic equations defined with respect to the planet inertial frame $M_1XYZ$ are given by [28, 29],

$$\dot{h} = V\sin\gamma, \tag{19}$$

$$\dot{V} = -\frac{C_D S}{m}\frac{\rho V^2}{2} - g\sin\gamma, \tag{20}$$

$$\dot{\gamma} = \left( \frac{V}{h + R_0} - \frac{g}{V} \right) \cos\gamma , \tag{21}$$

$$g = g_0 \left( \frac{R_0}{h + R_0} \right)^2 , \tag{22}$$

where $V$ is the velocity, $\gamma$ is the flight path angle, $g$ and $g_0$ are the gravitational acceleration at altitude $h$ and ground level ($h = 0$), respectively, and $R_0$ is the radius of planet.

To determine the initial conditions for equations (20)-(21) on the atmospheric part of the trajectory, the following equations for the transition from the frame $Oxy$ to the frame $M_1XY$ are used (Fig. 4)

$$X = \mu r + x\cos f - y\sin f , \tag{23}$$

$$Y = x\sin f + y\cos f . \tag{24}$$

Then, the altitude and velocity of the spacecraft and the flight path angle are written as,

$$h = \sqrt{X^2 + Y^2} - R_0 , \tag{25}$$

$$V = \sqrt{\dot{X}^2 + \dot{Y}^2} , \tag{26}$$

$$\gamma = \frac{\pi}{2} + (\alpha - \beta) , \tag{27}$$

where $\tan\alpha = \dfrac{Y}{X}$, $\tan\beta = \dfrac{\dot{Y}}{\dot{X}}$.

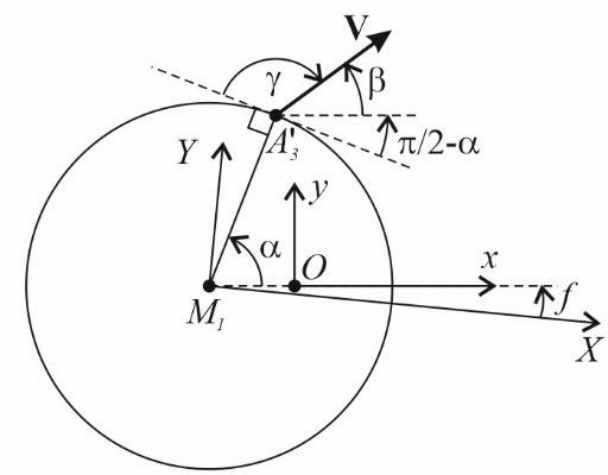


**Fig. 4.** The frame $Oxy$ and the frame $M_1XY$.

## 4. Two-impulse Phobos-Mars transfer

This section considers the two-impulse Phobos-Mars transfer. The entire transfer trajectory is divided into two parts: the launch trajectory and the landing trajectory which join at the transition point $A_2$. The simulation starts with the landing trajectory which leads to the determination of the position of the transition point $A_2$ on the axis $Ox$ that allows entry into the Martian atmosphere and subsequent landing on the Martian surface. In the second step, the launch trajectory is modeled to determine the acceleration ($\Delta V_1$) and deceleration ($-\Delta V_2$) velocity impulses that ensure hitting the transition point $A_2$.

### *4.1. The landing trajectory $A_2A_3$. Numerical simulation*

Conduct a numerical simulation using equations (17) and (18) for a spacecraft with ballistic coefficient $m/C_{\mathrm{D}}A = 100\ \mathrm{kg/m^2}$ in the Mars-Phobos system with the parameters given in Table 1. The system of equations is numerically integrated in

Wolfram Mathematica using a fifth-order Runge–Kutta method with a fourth-order error estimate and adaptive step size control based on the local error.

**Table 1.** Parameters of Moon-Planet systems environment.

| Description | Symbol | Value for Phobos-Mars | Value for Moon-Earth |
|---|---|---|---|
| Mass of the planet | $m_1$ | $6.417 \cdot 10^{23}$ kg | $5.9726 \cdot 10^{24}$ kg |
| Mass of the moon | $m_2$ | $1.072 \cdot 10^{16}$ kg | $3.3477 \cdot 10^{22}$ kg |
| Mass ratio | $\mu = m_2 / (m_1 + m_2)$ | $1.671 \cdot 10^{-8}$ | $5.5738 \cdot 10^{-3}$ |
| Planet's reference radius | $R_0$ | 3389.5 km | 6371.0 km |
| Semi-major axis of elliptical orbit | $a$ | 9377.2 km | 384748 km |
| Orbit eccentricity | $e$ | 0.015 | 0.055 |
| Atmospheric interface altitude | $h_A$ | 125 km | 100 km |
| Scale height | $h_s$ | 9354.5 m | 7000.0 m |
| Planet's surface atmospheric density | $\rho_0$ | 0.0158 kg m$^{-3}$ | 1.225 kg m$^{-3}$ |

Fig. 5 shows the three landing trajectories starting at the three different transition points $A_2$ and ending at the points $A_3$ on the planet's surface. The parameters required for constructing trajectories are given in Table 2. All landing

trajectories begins at the transition point $A_2$ on the axis at 50 km interval (Fig. 5). The entry velocity for all three trajectories is approximately $V_0 \approx 4.1\,\text{km/s}$, and the entry angles $\gamma_0$ vary from $-6°$ to $-12°$. The last three rows of Table 2 contain the time intervals obtained as a result of numerical simulation, in particular the duration of the atmospheric descent $t_{re}$, the duration of the orbital segment $t_{or}$ and the total maneuver time $t_2$. The orbital part of the landing trajectories lasts from 94 to 104 minutes, the atmospheric part lasts for 3 minutes on a steep trajectory (trajectory 3) and for 20 minutes on a gentle trajectory (trajectory 1). The maximum aerodynamic force acceleration on the gentle trajectory is 19.8 m/s$^2$ and on the steep trajectory is 65.5 m/s$^2$ (Fig. 6).

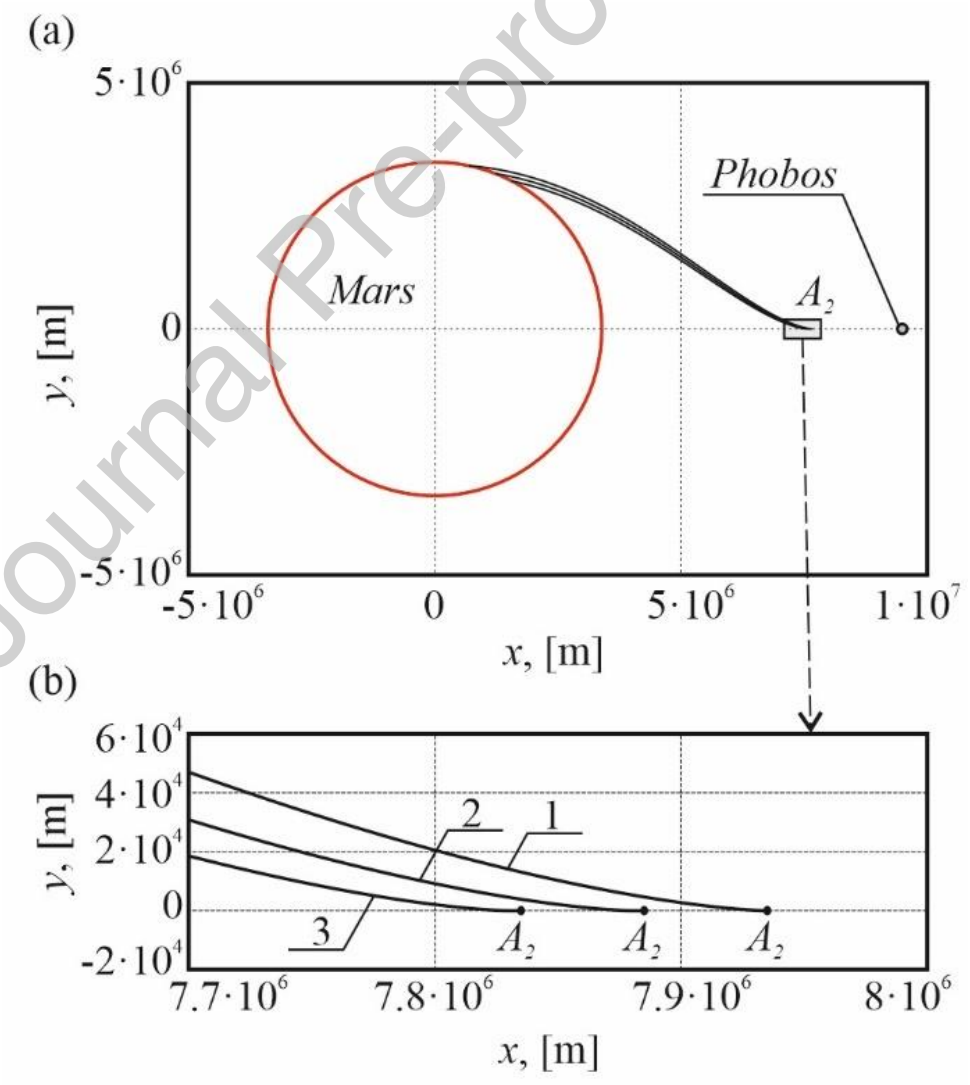

**Fig. 5** Landing trajectories from the transition point $A_2$ to reentry into the Mars atmosphere.

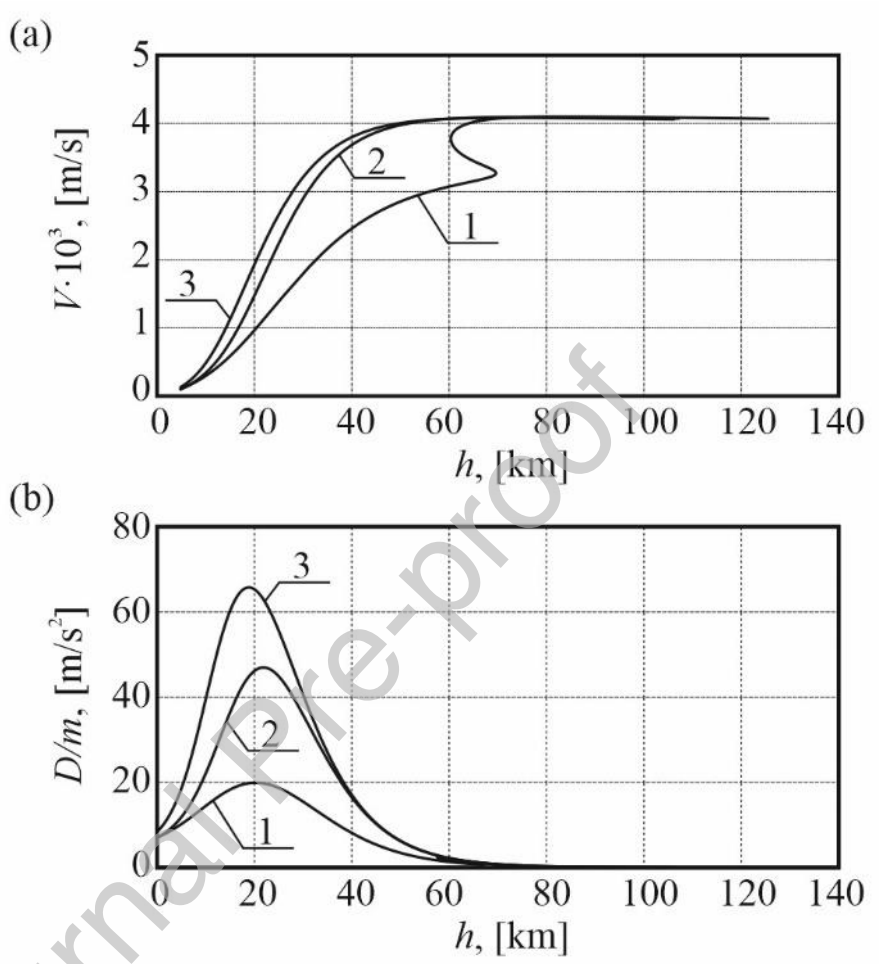




**Fig. 6.** The velocity (a) and the aerodynamic force acceleration (b).

**Table 2.** Mars atmospheric entry mission.

| Description | Symbol | Trajectory 1 | Trajectory 2 | Trajectory 3 |
|---|---|---|---|---|

| | | | | |
|---|---|---|---|---|
| Coordinate of point $A_2$ | $x_{A_2}$ | $7935 \cdot 10^3$ m | $7885 \cdot 10^3$ m | $7835 \cdot 10^3$ m |
| Altitude at the atmosphere edge | $h_0$ | 125 km | 125 km | 125 km |
| Initial velocity | $V_0$ | 4107 m/s | 4095 m/s | 4083 m/s |
| Initial flight path angle | $\gamma_0$ | –0.102rad | –0.171rad | –0.218rad |
| Maximum drag acceleration | $\max(D)/m$ | 19.8 m/s$^2$ | 47.1 m/s$^2$ | 65.5 m/s$^2$ |
| Re-entry time | $t_{\text{re}}$ | 1208 s | 243 s | 185 s |
| Orbital time | $t_{\text{or}}$ | 6214 s | 5890 s | 5641 s |
| Duration of landing trajectory | $t_2 = t_{\text{or}} + t_{\text{re}}$ | 7422 s | 6133 s | 5826 s |

*4.2. Backward integration method for plotting the launch trajectories*

The forward integration method is used above to plot the landing trajectories $A_2A_3$ from the initial transition point $A_2$. If the forward integration method is used to construct the launch trajectory $A_1A_2$, the 5 initial conditions for the system of the 5th order differential equations (5), (6) and (10) should be specified at the starting point. Even in the case when the position of launch point $A_1$ on the surface of Phobos is known, for example if it is the point just below the L1 libration point, there are only two initial coordinates $x_1$ and $y_1$. However, it is still necessary to specify the initial velocities $\dot{x}_1$ and $\dot{y}_1$ that make up the acceleration velocity impulse

$$\Delta V_1 = \sqrt{\dot{x}_1^2 + \dot{y}_1^2} \tag{28}$$

as well as the initial true anomaly $f_1$. Furthermore, the launch trajectory should take the spacecraft to a transition point $A_2(x_2, y_2)$, whose coordinates along with the value of the true anomaly $f_2$ are known. This is a very difficult problem because three values have be set at the launch point $A_1$:

$$\dot{x}(0) = \dot{x}_1, \quad \dot{y}(0) = \dot{y}_1, \quad f(0) = f_1, \tag{29}$$

so that three conditions are met at the transition point $A_2$:

$$\dot{x}(t_2) = \dot{x}_2, \quad \dot{y}(t_2) = \dot{y}_2, \quad f(t_2) = f_2, \tag{30}$$

where $t_2$ is the time duration of the launch trajectory. The deceleration velocity impulse should cancel the spacecraft velocity at the transition point $A_2$, i.e. it should be equal to

$$\Delta V_2 = \sqrt{\dot{x}_2^2 + \dot{y}_2^2} \quad . \tag{31}$$

To simplify the plotting of the launch trajectory that satisfies conditions (29) and (30), use the method of backward integration [26, 27]. This method allows us to integrate a new system of differential equations in the opposite direction from the transition point $A_2$ to the launch point $A_1$. The new system can be easily derived from the equations (5), (6), and (10) by substituting the independent variable $t = -\tau$, where $\tau$ is the new time variable. At such substitution, the first derivatives change the sign to the opposite one, and the second sign derivatives do not change

$$\dot{x} = -x', \; \dot{y} = -y', \; \ddot{x} = x'', \; \ddot{y} = y'', \; \dot{f} = -f', \tag{32}$$

where $()' = \frac{d}{d\tau}()$. As a result, we have the new equations for the backward integration

$$x'' - f'^2 x - 2 f' y' - f'' y = \frac{\partial U}{\partial x}, \tag{33}$$

$$y'' - f'^2 y + 2f'x' + f''x = \frac{\partial U}{\partial y}, \tag{34}$$

$$f' = -\frac{c}{r^2}. \tag{35}$$

Eqs. (33), (34), and (35) have the same trajectories in state space as the equations (5), (6), and (10). For the new equations at the transition point $A_2$, the true anomaly and coordinates are known. The two velocity projections have to be chosen to arrive at the launch point $A_1$, whose coordinates are given, and the initial true anomaly and velocity projections can be any. The problem is therefore much simpler, with only two parameters: $x'(\tau_2)$ and $y'(\tau_2)$ to choose and two conditions: $x(\tau_1)$ and $y(\tau_1)$ to satisfy, compared to the forward integration method.

*4.3. The launch trajectory $A_1A_2$. Numerical simulation*

Table 3 presents the parameters of the three launch trajectories starting from the launch point $A_1$ on the Phobos surface just below the L1 libration point and ending at different transition points 50 km apart.

**Table 3.** Launch from the Phobos surface.

| Description | Symbol | Trajectory 1 | Trajectory 2 | Trajectory 3 |
|---|---|---|---|---|
| Coordinate of point $A_2$ | $x_{A_2}$ | $7935 \cdot 10^3$ m | $7885 \cdot 10^3$ m | $7835 \cdot 10^3$ m |
| Initial coordinate | $x_0$ | $9477 \cdot 10^3$ m | $9477 \cdot 10^3$ m | $9477 \cdot 10^3$ m |
| Initial coordinate | $y_0$ | 0 | 0 | 0 |

| | | | | |
|---|---|---|---|---|
| Acceleration velocity impulse | $\Delta V_1$ | 308 m/s | 334 m/s | 344 m/s |
| Acceleration impulse angle | $\alpha_1$ | 1.452 rad | 1.318 rad | 1.314 rad |
| Deceleration velocity impulse | $\Delta V_2$ | 661 m/s | –694 m/s | –719 m/s |
| Deceleration impulse angle | $\alpha_2$ | –0.793 rad | –0.749 rad | –0.745 rad |
| Total velocity impulse | $\Delta V_1 + \Delta V_2$ | 969 m/s | 1028 m/s | 1053 m/s |
| Duration of launching trajectory | $t_1$ | 5230 s | 4780 s | 4760 s |
| Total time | $t_1 + t_2$ | 3.51 hours | 3.03 hours | 2.94 hours |

The launch trajectories in Fig. 7 are not optimal in terms of minimizing the total velocity impulse, let alone the only ones, but only one of the possible ones that illustrate the backward integration method.

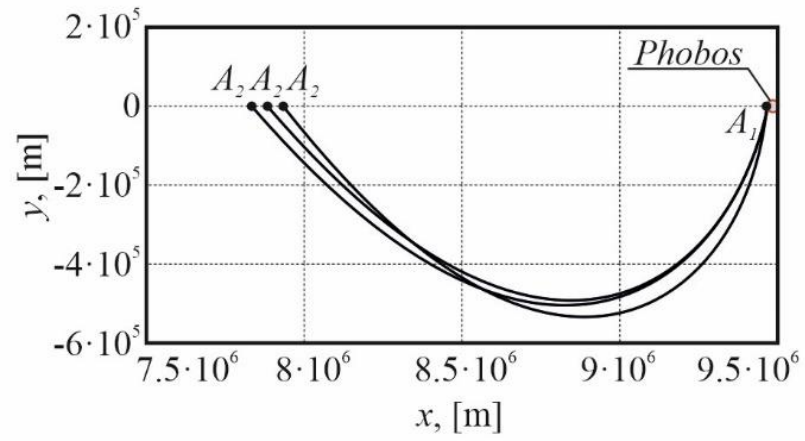

**Fig. 7.** The launch trajectories of the spacecraft from the launch point $A_1$ on Phobos to the transition point $A_2$.

## 5. Two-impulse Moon-Earth transfer

This section looks at the two-impulse transfer from the Moon to the Earth. In the Earth-Moon system ($\mu = 0.557 \cdot 10^{-2}$), the distance between the center of mass of the Earth and the center of mass of the Earth-Moon system is quite large ($\mu r > 2262$ km). In this case equations (19)-(21) are used to simulate the motion of the spacecraft in the atmosphere.

### *5.1. The landing trajectory $A_2A_3$. Numerical simulation*

For the simulation of motion, the Moon-Earth parameters are given in Table 1. Table 4 shows three landing trajectories. They start from three different transition points 500 km apart and end at the Earth's surface.

**Table 4.** Earth atmospheric entry mission.

| Description | Symbol | Trajectory 1 | Trajectory 2 | Trajectory 3 |
|---|---|---|---|---|
| Coordinate of point $A_2$ | $x_{A_2}$ | $150.5 \cdot 10^6$ m | $150.0 \cdot 10^6$ m | $149.5 \cdot 10^6$ m |
| Altitude at the atmosphere edge | $h_0$ | 100 km | 100 km | 100 km |
| Initial velocity | $V_0$ | 10793 m/s | 10792 m/s | 10791 m/s |

| | | | | |
|---|---|---|---|---|
| Initial flight path angle | $\gamma_0$ | –0.105 rad | –0.139 rad | –0.170 rad |
| Maximum drag acceleration | $\frac{\max(D)}{m}$ | 224 m/s$^2$ | 353 m/s$^2$ | 460 m/s$^2$ |
| Re-entry time | $t_{re}$ | 300 s | 290 s | 270 s |
| Orbital time | $t_{or}$ | 111959 s | 111307 s | 110661 s |
| Duration of landing trajectory | $t_2 = t_{or} + t_{re}$ | 112259 s | 111597 s | 110931 s |

Table 4 and Figs. 8 and 9 show that the entry velocity $V_0$ is approximately the same for all trajectories ($V_0 \approx 10.8$ km/s ), the entry angle $\gamma_0$ is $-6.0°$ for the gentle trajectory and increases to $-9.7°$ for the steep trajectory, resulting in an increase in the maximum drag acceleration from 224 m/s$^2$ to 460 m/s$^2$. The flight time from the intermediate point to landing on the Earth's surface is about 31 hours for all trajectories. Fig. 9 shows the change in the spacecraft velocity and the drag acceleration in the atmospheric section of the landing trajectory.

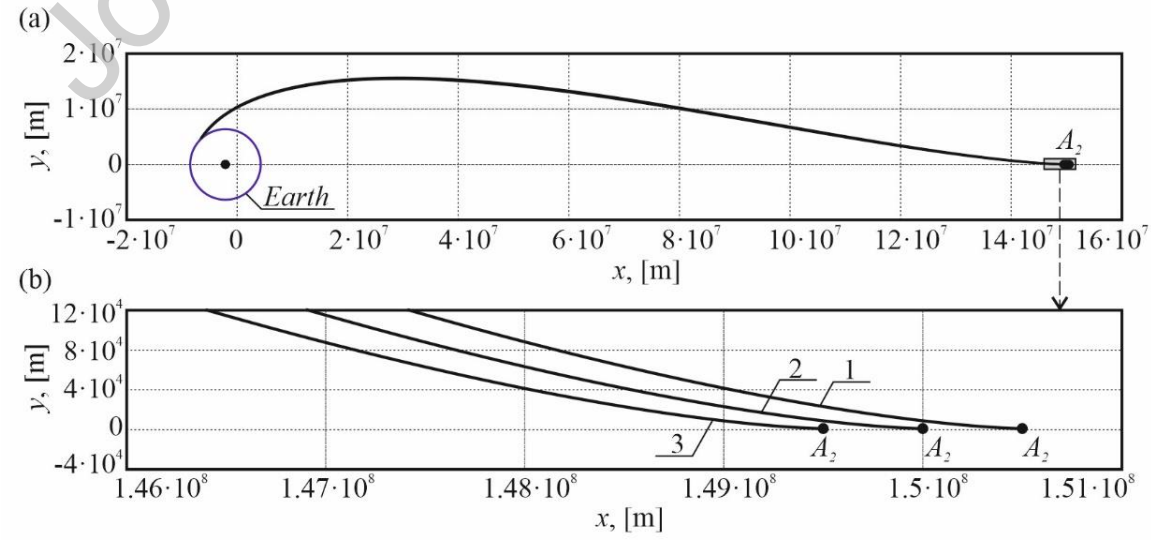

**Fig. 8.** Landing trajectories from the transition point $A_2$ to reentry into the Earth atmosphere.

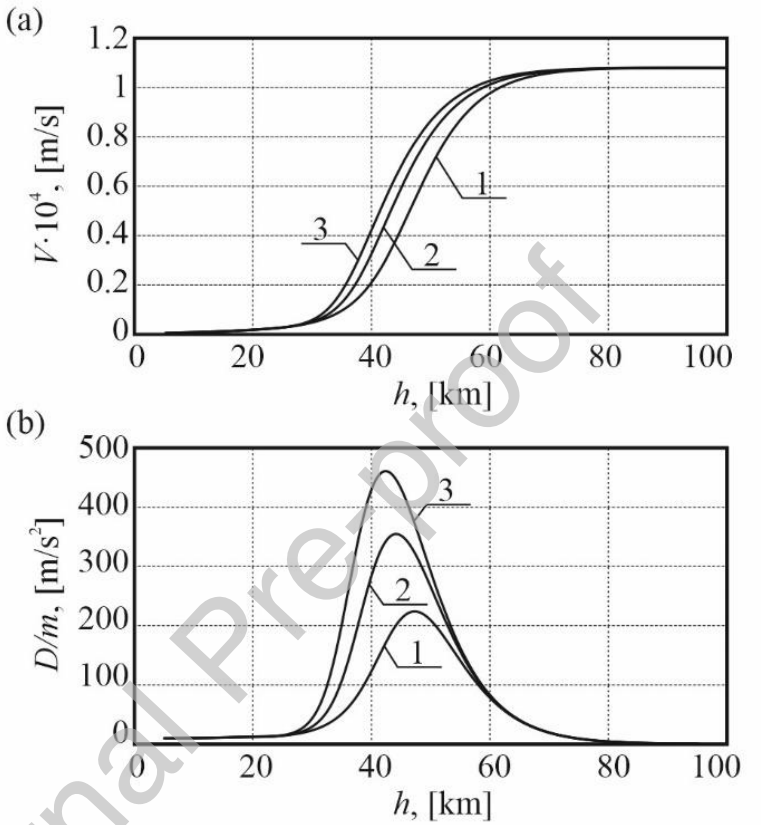


**Fig. 9.** The velocity (a) and the drag acceleration (b).

*5.2. The launch trajectory $A_1A_2$. Numerical simulation*

Consider the three landing trajectories described above, starting on the surface of the Moon directly below the $L_1$ libration point at the point $A_1$ and ending at the transition points located at 500 km intervals on the $Ox$ axis. The launch trajectories

are constructed using the backward integration method described in the subsection 4.2. Table 5 contains the values of the velocity impulses for these trajectories.

**Table 5.** Launch from the Moon surface.

| Description | Symbol | Trajectory 1 | Trajectory 2 | Trajectory 3 |
|---|---|---|---|---|
| Coordinate of point $A_2$ | $x_{A_2}$ | $150.5 \cdot 10^6$ m | $150.0 \cdot 10^6$ m | $149.5 \cdot 10^6$ m |
| Initial coordinate | $x_0$ | $379.7 \cdot 10^6$ m | $379.7 \cdot 10^6$ m | $379.7 \cdot 10^6$ m |
| Initial coordinate | $y_0$ | 0 | 0 | 0 |
| Acceleration velocity impulse | $\Delta V_1$ | 1064 m/s | 1045 m/s | 1051 m/s |
| Acceleration impulse angle | $\alpha_1$ | 1.016 rad | 1.025 rad | 1.038 rad |
| Deceleration velocity impulse | $\Delta V_2$ | 1700 m/s | 1700 m/s | 1700 m/s |
| Deceleration impulse angle | $\alpha_2$ | –0.5193 rad | –0.5226 rad | –0.5260 rad |
| Duration of launching trajectory | $t_1$ | $223.2 \cdot 10^3$ s | $225.5 \cdot 10^3$ s | $228.0 \cdot 10^3$ s |
| Total velocity impulse | $\Delta V_1 + \Delta V_2$ | 2763 m/s | 2745 m/s | 2751 m/s |
| Total time | $t_1 + t_2$ | 64.06 hours | 64.34 hours | 64.95 hours |

The launch trajectories in Fig. 10 are obtained by backward integration by selecting the end conditions at the transition points that ensure the start point is reached on the Moon's surface. These trajectories are not optimal in terms of minimising the total velocity impulse $\Delta V_\Sigma = \Delta V_1 + \Delta V_2$. For all three launch trajectories the total velocity impulse does not exceed the value of $\Delta V_\Sigma \le 2763$ m/s.

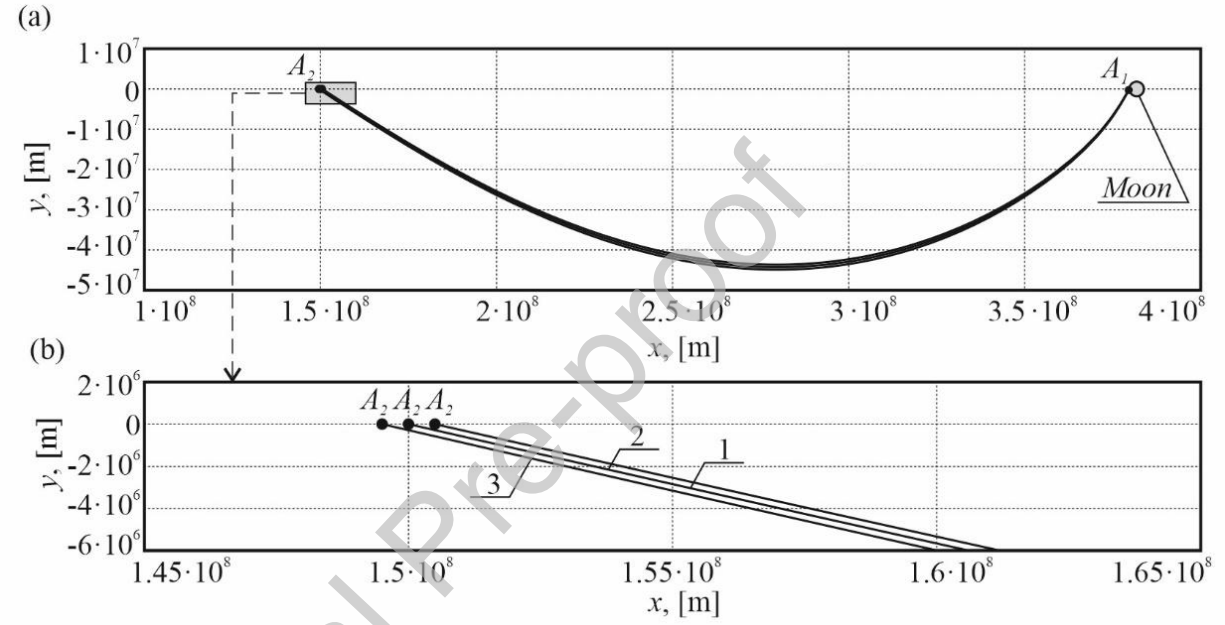


**Fig. 10.** The launch trajectories for the Moon-Earth transfer.



## 6. Conclusions

The results of numerical simulations allow us to highlight the advantages of the two impulse Moon-Planet flights. The proposed scheme allows the flight to be completed in a relatively short time. The total Moon-Earth transfer time is more than halved from 5.7 days for the classical Moon-Earth flight [7] to 2.7 days (Table 5), with comparable total velocity impulses of 2870 m/s [7] and 2763 m/s for the proposed scenario. The second advantage of the proposed scheme is its simplicity.

The proposed scenario requires only 2 engine firings compared to the classical scenario with 5 engine firings: 3 firings to reach the reference lunar orbit and one each for an acceleration impulse and for an orbit correction [7]. In addition, there is no need to change the direction of the thrust vector over time as in the classical scenario of insertion into a reference lunar orbit.

There are several issues to be discussed in the future. Is it possible to do a reverse two-impulse planet-moon transfer according to the scheme presented? This seems possible in principle, but needs to be confirmed by numerical modelling. The transition point $A_2$ should be located between the L1 libration point and the lunar surface. For the Earth-Moon system this distance is about 43000 km, then for the Mars-Phobos system it is only 3.4 km. In the first case it makes sense, in the second case it seems to make no sense at all at the transition point. Another question: what starting point on the lunar surface should we choose? In the paper, the lunar launch point $A_1$ is chosen to be below the L1 libration point. Such a launch point for Phobos is obviously the best candidate, since it is easiest to deliver something to the surface of Phobos at this point, using the L1 libration point to place the base spacecraft, as proposed for the PHLOTE mission [30]. There may be other options for the location of the launch point $A_1$ for the moon. It will be interesting to consider the proposed two-impulse transfer for other primaries' planet-moon systems, and investigate the problem of minimizing the total velocity impulse required to perform the proposed two-impulse transfer.



**Declaration of competing interest**

The authors declare that they have no known competing financial interests or personal relationships that could have appeared to influence the work reported in this paper.

**Acknowledgments**

I would like to thank Dr. Alexander Ledkov for helpful discussions of the simulation results.

**References**

[1] A.J. Schwaniger, Trajectories in the earth-moon space with symmetrical free return properties, 5 (1963). National Aeronautics and Space Administration.

[2] C. Uphoff, M.A. Crouch, Lunar cycler orbits with alternating semi-monthly transfer windows. Journal of the Astronautical Sciences, 41 (2) (1993) 189-205.

[3] E.E. Macau, Using chaos to guide a spacecraft to the moon. Acta Astronaut. 47 (12) (2000) 871-878. https://doi.org/10.1016/S0094-5765(00)00125-9.

[4] C. Du, L. Song, J. Zhang, Y. Liu, A novel calculation method for low-thrust transfer trajectories in the Earth-Moon restricted three-body problem. Aerospace Science and Technology. 147 (2024) 109048. https://doi.org/10.1016/j.ast.2024.109048.

[5] P. Grover, P., and Ross, S., "Designing Trajectories in a Planet-Moon Environment Using the Controlled Keplerian Map," J. Guid. Control Dynam. Vol. 32, No. 2, 2009, pp. 437–444. https://doi.org/10.2514/1.38320.

[6] C. Bao, J. Li, H. Baoyin, Two-segment lunar free-return trajectories design using the pseudostate theory. Advances in Space Research, 61 (1) (2018) 97–110, https://doi.org/10.1016/j.asr.2017.09.026.

[7] E.S. Gordienko A.V. Simonov, P.A. Khudorozhkov, Ballistic design of missions involving the delivery of Lunar soil to the Earth, Engineering Journal: Science and Innovation, 3 (99) (2020) 1-20 (in Russian), https://doi.org/10.18698/2308-6033-2020-3-1967.

[8] M. Lv, M. Tan, D. Zhou, Design of two-impulse Earth–Moon transfers using differential correction approach. Aerospace Science and Technology. 60 (2017) 183-192.

http://dx.doi.org/10.1016/j.ast.2016.11.008.

[9] D. Canales, K.C. Howell, E. Fantino, A versatile moon-to-moon transfer design method for applications involving libration point orbits. Acta Astronaut. 198 (2022) 388-402, https://doi.org/10.1016/j.actaastro.2022.06.010.

[10] D. Canales, M. Gupta, B. Park, K.C. Howell, A transfer trajectory framework for the exploration of Phobos and Deimos leveraging resonant orbits. Acta Astronaut. 194 (2022) 263-276.

https://doi.org/10.1016/j.actaastro.2022.02.00.

[11] D. Canales, K.C. Howell, E. Fantino, Transfer design between neighborhoods of planetary moons in the circular restricted three-body problem: the moonto-moon analytical transfer method, Celestial Mech. Dynam. Astronom. 133 (2021) 36.
http://dx.doi.org/10.1007/s10569-021-10031-x.

[12] A.N. Deutsch, J.W. Head, K.R. Ramsley, et al., Science exploration architecture for phobos and deimos: The role of phobos and deimos in the future exploration of mars, Adv. Space Res. 62 (8) (2018) 2174–2186.
http://dx.doi.org/10.1016/j.asr.2017.12.017.

[13] A. Farrés, C. Gao, J.J. Masdemont, G. Gómez, D.C. Folta, C. Webster, Geometrical analysis of station-keeping strategies about libration point orbits, J. Guid. Control Dynam. 45 (6) (2022) 1108-1125,

https://doi.org/10.2514/1.G006014.

[14] S.W. Yoon, V. Petukhov, Minimum-fuel low-thrust trajectories to the moon. Acta Astronaut. 210 (2023) 102-116,
https://doi.org/10.1016/j.actaastro.2023.05.006.

[15] J. Zhang, H. Yu, H. Dai, Overview of Earth-Moon Transfer Trajectory Modeling and Design. CMES-Computer Modeling in Engineering & Sciences, 135 (1) (2023) 1-43, https://doi.org/10.32604/cmes.2022.022585.

[16] D. Canales, K.C. Howell, E. Fantino, A.J. Gilliam, Transfers between moons with escape and capture patterns via Lyapunov exponent maps, J. Guid. Control Dynam. 46 (11) (2023), 2133-2149, https://doi.org/10.2514/1.G007195.

[17] Y. Wang, C. Han, X. Sun, Optimization of low-thrust Earth-orbit transfers using the vectorial orbital elements. Aerospace Science and Technology. 112 (2021) 106614. https://doi.org/10.1016/j.ast.2021.106614.

[18] D. Wang, D. Ye, Z. Sun, Shape-based method for low-thrust transfers between periodic orbits in cislunar space. Acta Astronaut. 219 (2024) 996-1006, https://doi.org/10.1016/j.actaastro.2024.03.016.

[19] Y. Qi, S. Xu, Earth–Moon transfer with near-optimal lunar capture in the restricted four-body problem. Aerospace Science and Technology. 55 (2016) 282-291. http://dx.doi.org/10.1016/j.ast.2016.06.008.

[20] J. Li, S. Gong, X. Wang, Analytical design methods for determining Moon-to-Earth trajectories. Aerospace Science and Technology. 40 (2015) 138-149. http://dx.doi.org/10.1016/j.ast.2014.10.016.

[21] W. Zhigang, W. Weiwei, L. Lu, L. Jiafu, Dynamic simulation of cargo transport along cislunar suspension tether by single node coupling model. Acta Astronaut. 226 (2025) 262-274, https://doi.org/10.1016/j.actaastro.2024.10.050.

[22] Y. Kayama, K.C. Howell, M. Bando, S. Hokamoto, Low-thrust trajectory design with successive convex optimization for libration point orbits, J. Guid. Control Dynam. 45 (4) (2022) 623-637, https://doi.org/10.2514/1.G005916.

[23] W. Hohmann, Die Erreichbarkeit der Himmelskörper, R. Oldenbourg, Munich, 1925 (in German). (The Attainability of Heavenly Bodies, NASA Technical Translation TTF44, Washington, DC, 1960.)

[24] V. Aslanov, An anchored space elevator under the L1 Mars-Phobos libration point. Acta Astronaut. (2025) In Press. https://doi.org/10.1016/j.actaastro.2025.05.032.

[25] V. Szebehely, The Restricted Problem of Three Bodies, Academic Press Inc., New York, 1967.

[26] T. Holzhüter, Optimal Regulator for the Inverted Pendulum via Euler–Lagrange Backward Integration. Automatica, 40 (9) (2004) 1613–1620. https://doi.org/10.1016/j.automatica.2004.04.012.

[27] H.K. Lee, K.W. Han, Analysis of Nonlinear Reactor Systems by Forward and Backward Integration Methods. IEEE Transactions on Nuclear Science, 47 (6) (2000) 2693–2698. https://doi.org/10.1109/23.901175.

[28] F.J. Regan, Dynamics of atmospheric re-entry. AIAA. 1993.

[29] N.X.Vinh, A. Busemann, R.D. Culp, Hypersonic and Planetary Entry Flight Mechanics, University of Michigan Press, Ann Arbor. 1980.

[30] K. Kempton, J. Pearson, E. Levin, J. Carroll, F. Amzajerdian, Phase 1 Study for the Phobos L1 Operational Tether Experiment (PHLOTE), End Report (2018) pp. 1–91. NASA, https://ntrs.nasa.gov/search.jsp?R=20190000916

**Declaration of Interest Statement**

☒ The authors declare that they have no known competing financial interests or personal relationships that could have appeared to influence the work reported in this paper.

☐ The author is an Editorial Board Member/Editor-in-Chief/Associate Editor/Guest Editor for this journal and was not involved in the editorial review or the decision to publish this article.

☐ The authors declare the following financial interests/personal relationships which may be considered as potential competing interests:

| |
|---|
| The author declare that there are no financial interests or personal relationships that could be considered as potential competing interests. |